

# Autonomous Recharging and Flight Mission Planning for Battery-operated Autonomous Drones

Rashid Alyassi\*, Majid Khonji\*, Sid Chi-Kin Chau, Khaled Elbassioni, Chien-Ming Tseng and Areg Karapetyan

**Abstract**—Unmanned aerial vehicles (UAVs), commonly known as drones, are being increasingly deployed throughout the globe as a means to streamline logistic and monitoring routines. When dispatched on autonomous missions, drones require an intelligent decision-making system for trajectory planning and tour optimization. Given the limited capacity of their onboard batteries, a key design challenge is ensuring the underlying algorithms can efficiently optimize the mission objectives along with recharging operations during long-haul flights. Against this backdrop, the present work undertakes a comprehensive study on automated management systems for battery-constrained drones: (1) We construct a machine learning model to estimate the energy expenditure of drones, considering diverse real-world factors and flight scenarios. (2) Leveraging this model, the joint problem of flight mission planning and recharging optimization is formulated as a multi-criteria combinatorial program aimed at completing a tour mission for a set of target sites in the shortest time while minimizing recharging duration. (3) We devise an efficient approximation algorithm, with provable near-optimal performance guarantees, and implement it in a drone management system, which supports real-time flight path tracking and re-computation in dynamic environments. (4) We validate the effectiveness and practicality of the proposed approach through extensive numerical simulations as well as real-world experiments.

**Index Terms**—Unmanned Aerial Vehicles, Flight Mission Planning, Recharging Optimization, Power Consumption Modeling.

## I. INTRODUCTION

In the near future, fully autonomous drones are expected for extensive deployment, giving rise to a new class of intelligent systems for logistics, wildlife surveillance, environmental surveying, search and rescue operations [1], [2]. Despite the popular applications in diverse sectors, the operations of drones are plagued with several challenges such as limited battery capacity [3]. Many drones are only suitable for short-range trips, which considerably limits their applicability. Another important challenge is due to dynamic operating environments. Drones are expected to travel within certain high altitudes and are significantly susceptible to wind and weather conditions. These conditions are highly dynamic and should be accounted for in a real-time manner. Furthermore, since drones are lightweight, the impact of wind is even more substantial.

This work was supported by the Khalifa University of Science and Technology under Award Ref. CIRA-2020-286.

R. Alyassi, M. Khonji, K. Elbassioni and A. Karapetyan are with the Department of Electrical Engineering and Computer Science, Khalifa University, Abu Dhabi, UAE. (e-mails: {rashid.alyassi, majid.khonji, khaled.elbassioni, areg.karapetyan}@ku.ac.ae)

S. C.-K. Chau is with the Australian National University. (e-mail: sid.chau@anu.edu.au). C.M. Tseng is with Ubiquiti Inc, Taiwan.

\*These authors contributed equally to the paper.

On the other hand, drones have several advantages over ground based transportation: (1) *Energy-efficiency*: Light-weight drones typically consume less energy per package-km than delivery trucks [3]. They are particularly energy-efficient for transporting light-weight items in short trips (within 4 km), whereas ground vehicles are useful for carrying heavier objects in long distance. (2) *Agility*: As there is little restriction in the sky, unlike on the ground with obstacles, drones can travel across space in straight paths, with nimble navigating ability. (3) *Swiftness*: Aerial transportation is usually not hampered by traffic congestions. Thus, the time to arrival is mostly reflected by the traveled distance. Drones can also be rapidly launched by catapults and drop-off payloads by parachutes with a short response time. (4) *Safeness*: As there is no on-board human operator, unmanned transportation missions are specially desirable in hazardous environments. In congested city environments, drone systems equipped with safety mechanisms, such as parachutes, can avoid or mitigate mid-air collisions as well as protect human users [4]. (5) *Low-cost*: Drone technologies have matured over time and price has dropped due to economies of scale. The use of customized drone systems can achieve better cost optimization in many application domains such as spraying fields, performing surveillance in precision agriculture, monitoring of difficult-to-access infrastructure, and delivering packages [5].

To improve the practical usefulness of autonomous drones, this paper presents several contributions to automated management systems for battery-operated drones:

- 1) We conduct empirical studies to model the power consumption of drones, considering various flight scenarios. Accurate model of battery performance in different scenarios allows further flight mission planning and recharging optimization for drones.
- 2) We formulate a joint problem of flight mission planning and recharging scheduling for drones, using a calibrated power consumption model of a drone. The objective is to complete a tour mission for a set of sites of interest in the shortest time, considering recharging possibilities. This problem captures diverse application domains such as logistics and remote surveillance.
- 3) We devise algorithms for solving the problem of flight mission planning and recharging scheduling. We subsequently implemented the algorithms in a drone management system, which supports real-time flight path tracking and re-computation in dynamic environments. Performance of the proposed approach is analytically established and experimentally corroborated.

- 4) To allow fully autonomous recharging of drones, we developed a robotic charging station prototype that can recharge drones in autonomous fashion.

## II. RELATED WORK

There are two main aspects of literature about drones: 1) low-level transient control of flight operations, for example, controlling propellers and balance using PID and MPC controllers [13], [14], and 2) high-level planning and management of drone missions, for example, obstacle avoidance, localization and mapping and trajectory planning [15]. However, the high-level studies typically focus on a single short-distance flight paths. Persistent long-distance flight mission planning involving multiple trips and recharging optimization has been considered to a lesser extent. Recently, several studies [7]–[12] considered mission planning problems for drones with different setups and scopes. However, these studies resort to heuristic-based approaches in solving the problem. On the other hand, this work provides more rigorous solution by an approximation algorithm with theoretically proven approximation guarantee. Table I provides a comparison of existing relevant literature along with our problem setting.

Arguably, drone platforms are energy efficient at certain tasks (e.g., package delivery), which offer an opportunity to enhance several existing sectors (e.g., logistics) [3]. Most prior studies of logistic optimization mainly focus on ground electric vehicles, not on aerial electric vehicles. Nonetheless, drones exhibit different characteristics that create some unique challenges. For example, the impact of wind is more substantial for drone flight. In [16], graph signal sampling and recovery techniques are used to plan routes for autonomous aerial vehicles, and a method is proposed to plan an energy-efficient flight trajectory by considering the influences of wind. Modeling and predicting electric vehicle power consumption has been the subject of a number of research papers. One method is the model-based whitebox approach, based on specific vehicle dynamics model to understand the consumption behavior of electric vehicles [17]. The power consumption estimation can also be obtained by a blackbox approach. For example, a general statistical approach using a regression model, without a vehicle dynamics model, can estimate the power consumption of vehicles [18]. The Blackbox model is more tractable and more convenient for trip optimization as it doesn't require detailed prior information on each drone in use and the operating environment. Hence, we will employ a similar blackbox model for aerial electric vehicles, but taking into account the flight conditions.

Over the last years, several general-purpose planners have emerged in the Artificial Intelligence (AI) community to address dynamic constraints for autonomous robots, like Kongming [19], COLIN [20] or ScottyActivity [21]. An important characteristic of COLIN's and ScottyActivity is that they do not require time discretization. This is essential for efficiently planning for typical scenarios with long horizons and activities with multiple time scales. Despite that ScottyActivity has significantly increased the expressivity of the problems that could be modeled, there is a lack of theoretical understanding

of solution quality and running time. These approaches often rely on heuristic forward search (HFS), such as in COLIN's and ScottyActivity's, and integer programming (IP), such as in p-Sulu [22], both of which are provably unscalable in many domains. This work explores a different approach by exploiting problem structure with a deeper understanding from a theoretical perspective. We extend several ideas from theoretical computer science literature and apply them to the problem of flight mission optimization, particularly considering battery-operated drones.

This work is related to the trip planning problem of electric vehicles [23]. There are recent results for path planning of electric vehicles considering recharging operations [24]. We adopt the solution proposed in [25] for the so-called tour gas station problem, for which efficient algorithms are designed for obtaining a near-optimal solution under certain assumptions. A variant of the classical algorithm [26] for the asymmetric travelling salesman problem (ATSP) was proposed in [6] for the tour gas station problem. In this work, we extend those methods to solve the problem for drone management by incorporating extensions to the settings of drone operations.

For fully autonomous drone management, drones should be able to recharge themselves without manual intervention. Inductive charging for drones has been proposed that can flexibly recharge drones in an autonomous manner [27]. However, this work relies on a different solution, with a combination of a robotic arm that can accommodate drone recharging in arbitrary positions and of varying drone sizes and shapes. To enable autonomous recharging of drones, an autonomous inductive charging system was initially proposed in [28], and is integrated with the management system of this paper.

## III. PROBLEM STATEMENT

This section formalizes the problem of joint flight mission planning and recharging optimization for battery-operated autonomous drones. We propose a multi-criteria objective function that seeks to complete a flight tour mission for a set of target sites in the shortest time while minimizing the duration of recharging operations. The underlying model involves multiple charging facilities and naturally captures diverse applications in logistic and monitoring systems.

As illustrated in Fig. 1, consider a set of sites of interest, denoted by  $\mathcal{S}$ , that a drone needs to visit (e.g., drop-off locations of parcels, or sites for measurements), and a set of charging station locations by  $\mathcal{C}$  where a drone can receive recharging. The base location of a drone is denoted by  $v_0$ . Let  $V \triangleq \mathcal{S} \cup \mathcal{C} \cup \{v_0\}$ .

Given a pair of locations  $(u, v) \in V$ , we denote the designated flight path by  $\ell(u, v)$ , and the flight time by  $\tau(u, v)$ . As is customary, we assume that while en route the drone first ascends vertically to a desired altitude, then travels in a straight path, and finally descends to the destination vertically. Let  $E(\ell(u, v), \tau(u, v))$  be the required energy consumption for the drone flying along  $\ell(u, v)$  within flight time  $\tau(u, v)$ . Here,  $E(\cdot, \cdot)$  is an increasing function that maps the combination of flight path  $\ell(u, v)$  and flight time  $\tau(u, v)$  to the required amount of energy. As exemplified in Section IV,  $E(\cdot, \cdot)$  can

	Problem Setup	Power Consumption Estimation	Recharging Optimization	Experimental Validation	Optimality Guarantees	Scope
Sundar and Rathinam (2013) [6]	Single UAV, multiple charging stations	X	X	X	✓	Mission planning
Dorling et. al. (2017) [7]	Multiple UAVs, single charging station	White-box model	X	✓	X	Multi-trip mission planning
Song et. al. (2018) [8]	Multiple UAVs, multiple charging stations	X	X	X	X	Multi-trip mission planning
Shao et. al. (2020) [9]	Multiple UAVs, multiple charging stations	X	X	X	X	Drone delivery routing
Ribeiro et. al. (2020) [10]	Multiple UAVs, multiple charging stations	X	X	X	X	Mission and charging station planning
Torabbeigi et. al. (2020) [11]	Multiple UAVs, single charging station	X	X	X	X	Mission planning
Cheng et. al. (2020) [12]	Multiple UAVs, single charging station	White-box model	X	X	X	Multi-trip mission planning
Present work	Single UAV, multiple charging stations	Black-box model	✓	✓	✓	Mission planning

TABLE I: A comparative summary of related literature on UAV routing and mission planning problems.

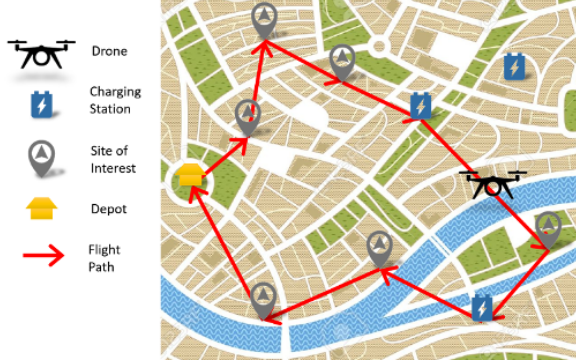


Fig. 1: A flight mission plan with recharging for a drone.

be estimated by a power consumption model of a drone. We represent the charging strategy by a function  $b(\cdot) : \mathcal{C} \mapsto \mathbb{R}$  that maps a charging station to an amount of energy to be recharged. When recharging its battery at  $u$ , let the incurred charging time be  $\tau_c(b(u))$ . Let  $\eta_c \leq 1$  and  $\eta_d \geq 1$  be the charging and discharging efficiency coefficients. Once at a charging station  $u \in \mathcal{C}$ , the drone recharges its battery by an amount of energy denoted by  $\eta_c b(u)$ . Whereas when flying between two sites  $u, v \in V$ , it consumes an amount of energy from the battery denoted by  $\eta_d E(\ell(u, v), \tau(u, v))$ .

We denote a *flight mission plan* by  $\mathcal{F}$ , which is a tour starting and terminating at  $v_0$ , consisting of a sequence of locations in  $\mathcal{S} \cup \mathcal{C} \cup \{v_0\}$ . Let  $\mathcal{F}_k$  be the  $k$ -th location in  $\mathcal{F}$ , then  $\mathcal{F}_1 = \mathcal{F}_{|\mathcal{F}|} = v_0$ . Let  $x_k$  be the state-of-charge (SoC) when reaching the  $k$ -th location  $\mathcal{F}_k$  in the flight mission plan. We require the SoC to stay within feasible range  $[\underline{B}, \bar{B}]$ . The lower bound of SoC,  $\underline{B}$ , ensures sufficient residual energy for the drone to return to the base, in case of emergency. We set the initial SoC  $x_0 = \bar{B}$ .

With the above notations, the drone flight mission planning with recharging problem (DFP) is formulated as:

$$(DFP) \quad \min_{\mathcal{F}, b(\cdot), x} \sum_{k=1}^{|\mathcal{F}|-1} \tau(\mathcal{F}_k, \mathcal{F}_{k+1}) + \sum_{k=1: \mathcal{F}_k \in \mathcal{C}} \tau_c(b(\mathcal{F}_k))$$

$$\text{s.t. } \mathcal{F}_1 = \mathcal{F}_{|\mathcal{F}|} = v_0 \quad (1)$$

$$\mathcal{S} \subseteq \mathcal{F} \subseteq \mathcal{S} \cup \mathcal{C} \cup \{v_0\} \quad (2)$$

$$x_k = \begin{cases} x_{k-1} - \Psi_{k,k+1}, & \text{if } \mathcal{F}_k \in \mathcal{S} \\ x_{k-1} + \eta_c b(\mathcal{F}_{k+1}) - \Psi_{k,k+1}, & \text{if } \mathcal{F}_k \in \mathcal{C} \end{cases} \quad (3)$$

$$\underline{B} \leq x_k \leq \bar{B}, \quad x_0 = \bar{B}, \quad (4)$$

where  $\Psi_{k,k+1} \triangleq \eta_d E(\ell(\mathcal{F}_k, \mathcal{F}_{k+1}), \tau(\mathcal{F}_k, \mathcal{F}_{k+1}))$ .

DFP aims to find a flight mission plan  $\mathcal{F}$  together with a charging strategy  $b(\cdot)$  that minimizes the total trip time, consisting of the flight time plus the recharging time, while maintaining the state-of-charge (SoC) within the operational

range. The difficulty of DFP is to balance the flight decisions and charging decisions. On one hand, a flight mission plan needs to consider the requirement of completing the mission in minimal total trip time. On the other hand, it needs to be able to reach a charging station, in case of insufficient battery, as well as minimizing the charging time.

The formulation of DFP can be extended to incorporate a variety of further factors for practical flight mission plan optimization, such as restrictions of no-fly zones and altitude, and wind speed forecast information. Users can also specify further goals, such as deadline of completion and maximum payload weight. An efficient optimization algorithm is required to compute an optimal flight mission plan to meet the users' specified goals. Further, DFP assumes constant weight throughout the flight mission. A more complicated problem with unloading payload at immediate sites will be a subject of future study.

#### IV. POWER CONSUMPTION MODEL

In order to accurately optimize the power consumption and flight missions of drones, we first conducted extensive experimentations to determine the battery performance of drones, considering various flight scenarios. In particular, we evaluate the power consumption using three commercial drone models, 3DR Solo [29], DJI Matrice 100 [30] and DJI Matrice 600 Pro [31], which appear in Fig. 2 (see Table IV in the Appendix for their specifications). The drones support developer kits, which allowed us to extract the sensor readings and program the flight paths. After gathering sufficient measurement data, we then apply regression models to capture the power consumption behavior of these drones.



Fig. 2: Left: 3DR Solo. Middle: DJI Matrice 100. Right: DJI Matrice 600 Pro.

#### A. Experimentation Settings and Scenarios

A typical drone is equipped with a number of sensors for two main purposes: (1) for self-stabilizing the drone in the air, and (2) for remotely tracking the drone status (e.g., the battery state-of-charge (SoC)). The stability of a drone is controlled by three essential sensors (i.e., gyroscopes, accelerometers and barometers), with which it can maneuver itself in the air. The SoC is measured by the voltage and current sensors. A major

part of power consumption of a drone is due to the powering of motors to lift itself in the air. Additional power consumption is required for the movements of the drone. The movements can be decomposed into vertical and horizontal directions. The barometer and GPS sensors can measure the 3-dimensional movements of a drone. The (ground) speed and position of a drone can be tracked by GPS and IMU modules, which also enable automatic navigation. The altitude of a drone can be tracked by barometer and GPS modules.

To understand the factors that determine the power consumption of a drone, we carried out the following experiments for obtaining empirical data in the rural areas, where the drone can fly in a straight path without obstacles:

- 1) *Impact of Motion*: The motions of a drone can be divided into three types: hovering, horizontal moving and vertical moving. We study the power consumption of a test drone in each motion type.
- 2) *Impact of Weight*: Typical drones can carry extra payloads, such as camera equipment or parcels. We study the impact of different weights of payloads attached to a test drone.
- 3) *Impact of Wind*: The major environmental factor that affects the drone is wind, including wind direction and ground speed. Wind may benefit the power consumption in some cases, as well as incurring resistance to the movement in other cases. We study the power consumption of a test drone in various wind conditions.

The experimental results are described as follows.

1) *Impact of Motion*: To study the power consumption of motions of a drone, we conducted four experiments. The battery power, barometer and GPS location, and ground speed data were collected in the first three experiments to analyze the performance of test drone 3DR Solo. The fourth experiment depicted the relation between horizontal movement and payload of the DJI Matrice 600 drone.

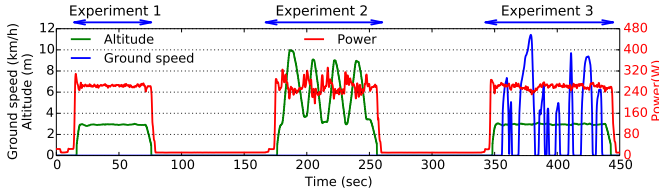


Fig. 3: Motion and battery power consumption of 3DR Solo.

Fig. 3 depicts the recorded data traces of three experiments of a test drone. We discuss several observations as follows:

- *Experiment 1*: The test drone hovered in the air without any movement in this experiment. Note that the drone may slightly drift around the takeoff location due to deviation error of GPS modules. We filter the speed data that is smaller than 0.5 m/s. This experiment shows the baseline power consumption of this flying drone. From the recorded data, we observe that the drone can maintain a sufficiently steady flying altitude with steady power consumption.
- *Experiment 2*: The test drone ascended and descended repeatedly in this experiment. The barometer data shows the altitude of the drone. The time series data allow

us to compute the vertical acceleration and speed of the drone. We observe larger power fluctuations due to repeatedly vertical movements. Power consumption increases slightly, when the drone ascends steady.

- *Experiment 3*: The test drone moved horizontally without altering its altitude in this experiment. The GPS data comprises of speed and course angle of the drone. We also gathered average wind speed and direction using a wind speed meter during the experiment. We observe smaller power fluctuations due to horizontal movements. We also measure idle power consumption of the drone between the two experiments.

2) *Impact of Weights*: One of the practical purposes of drones is to deliver payloads, and hence, the total weight of a drone varies with the payload it carries. We carried out several experiments with different weights of payloads on the test drone 3DR Solo to obtain empirical data. Three different weights were tested on the drone. The drone was set to hover in the air without any movement to obtain the corresponding baseline power consumption.

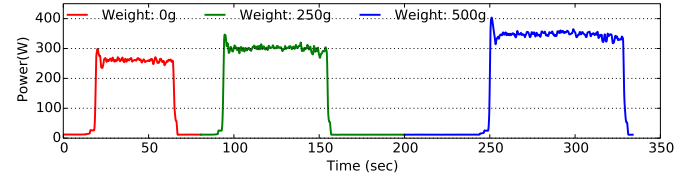


Fig. 4: Battery power consumption of test drone 3DR Solo with different payload weights.

Fig. 4 depicts the battery power consumption of 3DR Solo carrying three different weights. We observe that power consumption increases almost linearly when the weight of payload increases. The weight limit of payload depends on the thrusts that the motors can produce. Note that the maximum payload weight is 500g for 3DR Solo.

We observed a similar pattern with a heavier drone, DJI Matrice 600, and heavier payloads. In Fig. 5, the drone moves horizontally without altering its altitude under three different speed and payload profiles. We observe almost constant power consumption under different horizontal speeds, while horizontal acceleration has higher consumption with heavier payloads.

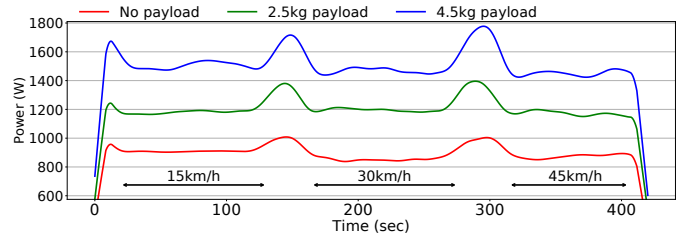


Fig. 5: Power consumption of DJI Matrice 600 under different payloads and horizontal speeds.

3) *Impact of Wind*: Wind condition is a major environmental factor to affect the power consumption of test drone 3DR Solo. We conducted several experiments under different wind conditions: *headwind* by flying against the direction of wind, and *tailwind* by flying along the direction of wind. The experiments were carried out at the same location but on different days with different wind conditions. The wind

directions and average speeds were measured using a wind speed meter for each experiment. Once the wind direction was determined, the drone was set to fly into a headwind or tailwind at maximum ground speed (18 km/h).

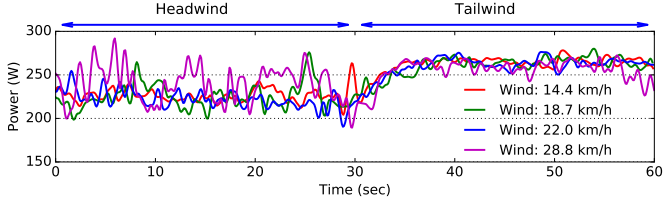


Fig. 6: Battery power consumption of 3DR Solo under different wind conditions.

Fig. 6 depicts the battery power consumption of 3DR Solo under different wind conditions. We observe smaller power consumption when flying into headwind, which is due to the increasing thrust by *translational lift*, when the drone moves from hovering to forward flight. When flying into a headwind, translational lift increases due to the relative airflow over the propellers increases, resulting in less power consumption to hover the drone [32]. However, when the wind speed exceeds a certain limit, the aerodynamic drag may outweigh the benefit of translational lift. In our setting, the drone speed is relatively slow, even at maximum speed. Hence, flying into a headwind is likely more energy-efficient.

### B. Regression Model of Power Consumption for Drones

Since typical drones are aerial electric vehicles, we can apply the methodology from the literature of general electric vehicles to model the power consumption of a drone. There are two main types of power consumption models of a drone:

- **White-box Model:** A straightforward approach is to employ a white-box microscopic behavior model for each drone that comprehensively characterizes the motor performance, aerodynamic environment, and battery systems. However, such a white-box model requires a large amount of data for calibration and detailed knowledge specific to a particular drone. For example, the aerodynamic parameters such as propeller efficiencies, motor efficiencies and drag coefficients are difficult to obtain accurately without resorting to sophisticated experimental setups like wind tunnel.
- **Blackbox Model:** A blackbox approach is more desirable, because it requires minimal knowledge of vehicle model with only a small set of measurable variables and parameters of the drone. In the subsequent sections, a blackbox model of power consumption of a drone will be utilized for flight mission planning and recharging optimization. The advantage of blackbox model is that it is obtained from simple data measurements without relying on sophisticated experimental setups.

This section describes a general multivariate blackbox model of power consumption for a drone that has been used extensively in the literature of electric vehicles [18], [33]–[36], which will be verified in the later empirical studies.

Let the estimated battery power consumption of a drone be  $\hat{P}$ , which is estimated by a number of measurement parameters in the following linear equation:

$$\hat{P} = \begin{bmatrix} \beta_1 \\ \beta_2 \\ \beta_3 \end{bmatrix}^T \begin{bmatrix} \|\vec{v}_{xy}\| \\ \|\vec{a}_{xy}\| \\ \|\vec{v}_{xy}\| \|\vec{a}_{xy}\| \end{bmatrix} + \begin{bmatrix} \beta_4 \\ \beta_5 \\ \beta_6 \end{bmatrix}^T \begin{bmatrix} \|\vec{v}_z\| \\ \|\vec{a}_z\| \\ \|\vec{v}_z\| \|\vec{a}_z\| \end{bmatrix} + \begin{bmatrix} \beta_7 \\ \beta_8 \\ \beta_9 \end{bmatrix}^T \begin{bmatrix} m \\ \vec{v}_{xy} \cdot \vec{w}_{xy} \\ 1 \end{bmatrix} \quad (5)$$

where

- $\vec{v}_{xy}$  and  $\vec{a}_{xy}$  are the speed and acceleration vectors describing the horizontal movement of the drone.
- $\vec{v}_z$  and  $\vec{a}_z$  are the speed and acceleration vectors describing the vertical movement of the drone.
- $m$  is the weight of payload.
- $\vec{w}_{xy}$  is the vector of wind movement in the horizontal surface.
- $\beta_1, \dots, \beta_9$  are the coefficients, and  $\|\vec{v}\|$  denotes the magnitude of a vector.

The coefficients  $\beta_1, \dots, \beta_9$  can be estimated by the standard regression method, if sufficient measurement data is collected.

Assuming the uniform conditions (e.g., speed, wind) within a period of duration  $D$ , the total energy consumption of the drone in duration  $D$  is estimated by  $\hat{P} \cdot D$ . We note that while this model does not capture all detailed factors, it can provide relatively accurate estimation of battery energy consumption with low complexity.

### C. Evaluation of Power Consumption Model

To evaluate the accuracy of the power consumption model, we conducted experiments to collect extensive empirical data to estimate the corresponding coefficients. Three test drones (3DR Solo, DJI Matrice 100 and DJI Matrice 600) were used in two sets of experiments. A test drone was programmed to first fly vertical movements, then flying into a headwind and a tailwind with different weights of payloads. The drone maintained its altitude during the horizontal flight. We conducted experiments under simple conditions, where the drone ascended from the source until reaching the desired altitude and then flew directly to the destination without changing its altitude. But the experiments are sufficiently representative of other conditions. The estimated coefficients of power consumption models for 3DR Solo, DJI Matrice 100 and Matrice 600 are:  $\beta_{\text{solo}} = [-2.595, 0.116, 0.824, 18.321, 31.745, 13.282, 0.197, 1.43, 251.7]$ ,  $\beta_{\text{m100}} = [-1.526, 3.934, 0.968, 18.125, 96.613, -1.085, 0.220, 1.332, 433.9]$ , and  $\beta_{\text{M600}} = [-1.777, 4.408, -0.038, 93.94, 1.362, -0.111, 140.46, 2.249, 0.0]$ .

We discussed the evaluation results of the test two drones using ground truth power consumption data. Fig. 7 presents the results for 3DR Solo, whereas Fig. 8 present the results for DJI Matrice 100. Fig. 7 and Fig. 8 depict the collected sensor data of our experiments for 3DR Solo and DJI Matrice 100, respectively, along with estimated power consumption. We tested three different weights of payloads under similar flight trajectories in each set of experiments. We obtain the estimated power consumption using the respective regression model and compare it to the ground truth power consumption data. We observe that the estimation is close to the actual measurement

data. The errors of estimation of power consumption in the experiments are within 0.4%, showing relatively good accuracy of our power consumption models for both test drones. We observed a similar pattern with DJI Matrice 600.

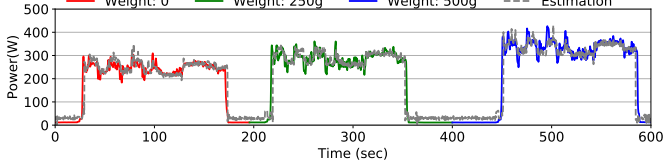


Fig. 7: Sensor data and estimation of 3DR Solo.

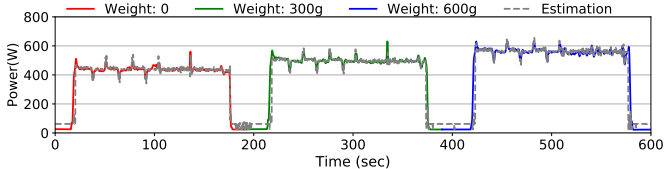


Fig. 8: Sensor data and estimation of DJI Matrice 100.

## V. SOLUTION METHODOLOGY

### A. Case with Uniform Drone Speed and Steady Wind Condition

To provide efficient algorithms for DFP, we first consider a basic setting under some realistic assumptions. Suppose that the horizontal speed of the drone is a uniform constant under steady wind condition, which will be relaxed in Sec. V-B. Then, the flight time  $\tau(u, v)$  between two sites  $u, v \in \mathcal{V}$  is proportional to the length of flight path  $\ell(u, v)$ , denoted by  $d(u, v)$ . Our regression model of energy consumption for drone in Sec. IV implies that the function  $E(\ell(u, v), \tau(u, v))$  is linear in the distance  $d(u, v)$ , and the charging time  $\tau_c(b(u))$  is linear in the amount of recharged energy  $b(u)$ . Thus, we assume the following linear objective functions:

$$\tau(u, v) = c_a d(u, v), \quad \tau_c(b(u)) = c_b b(u), \quad (6)$$

$$E(\ell(u, v), \tau(u, v)) = c_f(u, v) \cdot d(u, v), \quad (7)$$

for some constants  $c_a, c_b, c_f(u, v) > 0$ . Note that we allow  $c_f(u, v)$  to be edge-dependent. This can model non-uniform environment<sup>1</sup> for each  $\ell(u, v)$ , for instance, a path experiencing stronger wind is expected to have a larger constant  $c_f(u, v)$ . Denote the lower and upper bounds of  $c_f$  by  $\underline{c}_f \triangleq \min_{(u, v)} c_f(u, v)$  and  $\bar{c}_f \triangleq \max_{(u, v)} c_f(u, v)$ .

In this paper, we consider mostly long-distance trips (e.g., 2-3 km), for which the vertical landing and take-off operations (e.g., < 10m vertically) usually constitute a small part of the whole flight, and consume only a small percentage of the total energy (e.g., < 1%). For clarity of presentation, we assume that the energy consumption of landing and take-off operations is implicitly captured by  $c_f(u, v) \cdot d(u, v)$ , though our results can be easily extended to consider that explicitly.

For convenience of notation, for a flight mission plan  $(\mathcal{F}, b(\cdot))$ , we write  $\tau(\mathcal{F}) \triangleq \sum_{k=1}^{|\mathcal{F}|-1} \tau(\mathcal{F}_k, \mathcal{F}_{k+1})$  and  $b(\mathcal{F}) \triangleq \sum_{k=1}^{|\mathcal{F}|} \tau_c(b(\mathcal{F}_k))$ . Also, define  $d(\mathcal{F}) \triangleq \sum_{k=1}^{|\mathcal{F}|-1} d(\mathcal{F}_k, \mathcal{F}_{k+1})$ .

<sup>1</sup>Note that we implicitly consider the asymmetry in the energy consumption function, due to wind direction, by assuming two different constants  $c_f(u, v)$  and  $c_f(v, u)$ .

Under the aforementioned assumptions, the total charging time  $\tau_c(b(\mathcal{F}))$ , in an optimal flight mission plan  $\mathcal{F}$ , is related to the total flight time  $\tau(\mathcal{F})$  by the following lemma.

**Lemma 1.** *In an optimal flight mission plan  $(\mathcal{F}, b(\cdot))$ , we have*

$$c \cdot d(\mathcal{F}) + c' \leq \tau(\mathcal{F}) + \tau_c(b(\mathcal{F})) \leq \bar{c} \cdot d(\mathcal{F}) + c'$$

where either

- 1)  $\underline{c} = \bar{c} = c_a$  and  $c' = 0$ , or
- 2)  $\underline{c} = c_a + \underline{c}_f c_b \frac{\eta_d}{\eta_c}$ ,  $\bar{c} = c_a + \bar{c}_f c_b \frac{\eta_d}{\eta_c}$ , and  $c' = \frac{c_b}{\eta_c} (\bar{B} - x_0)$ .

*Proof.* See the Appendix.  $\square$

Lemma 1 characterizes the total charging time with respect to total fight time in the optimal flight plan by the respective upper and lower bounds in terms of the distances to be traveled.

**Lemma 2.** *Given any feasible flight mission plan  $(\mathcal{F}, b(\cdot))$ , there is another feasible flight mission plan  $(\mathcal{F}, b'(\cdot))$  such that*

$$\tau_c(b(\mathcal{F})) \leq \frac{\bar{B} - x_0}{\eta_c} + \frac{\bar{c}_f \eta_d}{\eta_c} \cdot d(\mathcal{F})$$

Such a plan  $(\mathcal{F}, b'(\cdot))$  can be found in  $O(|V|)$  time.

*Proof.* See the Appendix. (Algorithm 4 below shows how to construct such a plan explicitly.)  $\square$

Both Lemma 1 and Lemma 2 allow us to focus on minimizing the distance  $d(\mathcal{F})$  instead of total trip time. Hence, we simplify the problem DFP as a simplified formulation (SDFP), such that its optimal solution is later shown to be within a constant factor with an optimal solution of DFP. The simplified formulation (SDFP) is defined as follows.

$$(SDFP) \quad \min_{\mathcal{F}, x} \sum_{k=1}^{|\mathcal{F}|-1} \widehat{d}(\mathcal{F}_k, \mathcal{F}_{k+1}) \quad (8)$$

$$\text{s.t. } \mathcal{F}_1 = \mathcal{F}_{|\mathcal{F}|} = v_0 \quad (9)$$

$$\mathcal{S} \subseteq \mathcal{F} \subseteq \mathcal{S} \cup \mathcal{C} \cup \{v_0\} \quad (10)$$

$$x_k = \begin{cases} x_{k-1} - \eta_d \widehat{d}(\mathcal{F}_k, \mathcal{F}_{k+1}), & \text{if } \mathcal{F}_k \in \mathcal{S} \\ \bar{B}, & \text{if } \mathcal{F}_k \in \mathcal{C} \end{cases} \quad (11)$$

$$\underline{B} \leq x_k \leq \bar{B}, \quad x_0 = \bar{B} \quad (12)$$

In SDFP, we consider a modified distance function  $\widehat{d}(\cdot, \cdot)$ , which is defined as follows. Recall that  $V \triangleq \mathcal{S} \cup \mathcal{C} \cup \{v_0\}$ . Consider a weighted directed complete graph  $G_0 = (V, 2\binom{|V|}{2})$ , whose edge lengths are defined by  $\{c_f(u, v) \cdot d(u, v)\}_{u, v}$ . Then, obtain  $\{\widehat{d}(u, v)\}_{u, v}$ , which are the pairwise shortest distances of each pair of nodes in  $G_0$ . SDFP is related to the *tour gas station problem* in [25], which optimizes a tour trip of a vehicle in minimal fuel cost, with options of refilling at given gas stations.

Note that we assume in the formulation of SDFP that the SoC is brought to its maximum at each charging station. Once we obtain a tour under this assumption, it can be turned into a flight mission plan with the minimal charging requirements using Lemma 2.

For  $u \in V$ , let  $d'_u \triangleq \min_{v \in \mathcal{C}} \widehat{d}(u, v)$  be the distance to the nearest charging station from  $u$ , and  $s'_u \triangleq \operatorname{argmin}_{v \in \mathcal{C}} \widehat{d}(u, v)$

be the corresponding nearest charging station from  $u$ . And let  $d''_u \triangleq \min_{v \in \mathcal{C}} \hat{d}(v, u)$  be the shortest distance starting from a charging station to  $u$ , and  $s''_u \triangleq \operatorname{argmin}_{v \in \mathcal{C}} \hat{d}(v, u)$  be the corresponding charging station. Since we have asymmetric distances,  $s'_u$  is not necessarily equal to  $s''_u$ .

Define  $U \triangleq \frac{\bar{B} - \underline{B}}{\eta_d}$ . Following [25], we make a mild assumption that for every  $u \in \mathcal{S} \setminus \{v_0\}$  there is  $v \in \mathcal{C}$  such that  $d(u, v) \leq \alpha \frac{U}{2}$ , where  $\alpha \in [0, 1]$ . Intuitively, this assumption indicates that the distance between a pair of sites is always reachable by the available battery capacity. This assumption can be justified (for  $\alpha = 1$ ) as follows. For a location  $u \in \mathcal{S} \setminus \{v_0\}$ , if every  $v \in \mathcal{C}$  is at distance greater than  $\frac{U}{2}$ , then it is infeasible to visit  $u$  without incurring the battery level below  $\underline{B}$  (as the SoC drops below  $\bar{B} - \eta_d U = \underline{B}$ ). Moreover,  $\beta$  is defined as the maximum ratio between edges going between two gas stations, such as  $d(u, v) \leq \beta \cdot d(v, u) \quad \forall u, v \in D$ .

In the following, we present an algorithm to SDFP and then DFP. The main algorithm is  $\text{Find-plan}[V, d]$ , which is an extension of the Hungarian Algorithm [26], for finding a tour for asymmetric travelling salesman problem, and the results in [6]. It converts the graph into a bipartite graph, iteratively solves the minimum assignment problem, and finally combines all sub-tours to get a single tour. The resulting tour is passed to the procedure  $\text{Fix-plan}$  for converting it to a feasible flight mission plan  $\mathcal{F}$ , which might use a non-optimal charging function  $b(\cdot)$ . Then, the resulting plan  $(\mathcal{F}, b(\cdot))$  is further passed to procedure  $\text{Fix-charge}$  for finding the minimal charging requirements with respect to the flight mission plan  $\mathcal{F}$ . Specifically, the three procedures in  $\text{Find-plan}[V, d]$  are:

- $\text{Init-distances}[V, \hat{d}, u, v]$ : This provides a lower bound for an optimal solution. Namely, it finds for every pair of locations  $u, v \in V$ , the minimum possible distance  $\hat{d}(u, v)$ , and the corresponding shortest path  $\mathcal{P}(u, v)$  to go from  $u$  to  $v$  without going out of the operational range of the battery. Note that if  $\hat{d}(u, v) \leq U - d''_u - d'_v$  then the drone can always go directly from  $u$  to  $v$ <sup>2</sup>. Otherwise, at best (in an optimal solution), the drone can reach  $u$  with SoC at most  $\bar{B} - \eta_d d''_u$ , then it can visit a sequence of charging stations (only if the distance  $\hat{d}$  between two successive such stations is at most  $U$ ), then, from the last station, it has to reach  $v$  such that the SoC at  $v$  is at least  $\underline{B} + \eta_d d'_v$  (so that there is sufficient battery to reach  $s_v$ ). In particular, the distance from  $u$  to the first charging station on this path should be at most  $U - d''_u$ . Similarly, the distance from the last station on the path to  $v$  should be at most  $U - d'_v$ . This explains the definition of the graph  $G$  in line 5 of the procedure.
- $\text{Fix-plan}[G, \mathcal{F}_0]$ : starting from the flight mission plan  $\mathcal{F}_0$  obtained using the (modified) Hungarian algorithm [26] with respect to the weights  $\hat{d}$ , this procedure reconstructs a feasible flight mission plan  $\mathcal{F}$  for problem (SDFP). It first replaces each edge  $(u, v)$  in the flight mission plan by the corresponding path  $\mathcal{P}(u, v)$ . Since

<sup>2</sup>That is, starting with SoC =  $\bar{B}$  at  $s_u$ , then the drone reaches  $u$  with SoC  $\bar{B} - \eta_d d''_u$ , and then it flies directly from  $u$  to  $v$  causing the SoC to drop to  $\bar{B} - \eta_d(d''_u + \hat{d}(u, v)) = \underline{B} + \eta_d(U - d''_u - \hat{d}(u, v)) \geq \underline{B} + \eta_d d'_v$  at  $v$ . Thus, there is sufficient battery at  $v$  to reach  $s_v$ .

the resulting flight mission plan maybe still infeasible, the procedure adds to every site a round trip to closest charging station from the side and closest charging station to the site. Finally, the added stations are dropped one by one in a greedy way as long as feasibility is maintained.

- $\text{Fix-charge}[\mathcal{F}, b(\cdot)]$ : Starting from the flight mission plan  $(\mathcal{F}, b(\cdot))$  constructed after calling procedure  $\text{Fix-plan}[G, \mathcal{F}_0]$ , this procedure finds a minimal amount of recharging energy, according to Lemma 2.

Let  $\text{OPT}_{\text{DFP}}$  and  $\text{OPT}_{\text{SDFP}}$  be the optimal solutions of problems (DFP) and (SDFP), respectively.

**Lemma 3** ([6]). *The flight mission plan  $\mathcal{F}$  returned by algorithm  $\text{Find-plan}[V, d]$  has cost  $\hat{d}(\mathcal{F}) \leq \left( \frac{(1+\alpha+\alpha\beta)\log(|T|)}{1-\alpha} \right) \text{OPT}_{\text{SDFP}}$ .*

The following theorem establishes that algorithm  $\text{Find-plan}[V, d]$  has an asymptotic constant-factor approximation guarantee for DFP.

**Theorem 1.** *The flight mission plan  $(\mathcal{F}, b'(\cdot))$  returned by algorithm  $\text{Find-plan}[V, d]$  has cost*

$$\tau(\mathcal{F}) + \tau_c(b(\mathcal{F})) = O(\text{OPT}_{\text{DFP}}) + O(1).$$

*Proof.* See the Appendix.  $\square$

---

### Algorithm 1 Find-plan $[V, d]$

---

```

1: Compute pairwise shortest distances  $\{\hat{d}(u, v)\}_{u,v}$  on weighted directed
graph  $G_0 = (V, 2(V \choose 2))$ 
2: for each  $u, v \in V$  do
3:    $(\hat{d}(u, v), \mathcal{P}(u, v)) \leftarrow \text{Init-distances}[V, \hat{d}, u, v]$ 
4: end for
5: Consider the weighted directed graph  $G = (V, E; \hat{d})$  where  $E = 2(V \choose 2)$ 
6:  $\mathcal{F}_0 \leftarrow$  find a tour using the Hungarian algorithm on  $G$ 
7:  $\mathcal{F} \leftarrow \text{Fix-plan}[G, \mathcal{F}_0]$ 
8:  $b'(\cdot) \leftarrow \text{Fix-charge}[\mathcal{F}, b(\cdot)]$ 
9: return  $(\mathcal{F}, b'(\cdot))$ 

```

---

### Algorithm 2 Init-distances $[V, \hat{d}, u, v]$

---

```

1: if  $\hat{d}(u, v) \leq U - d''_u - d'_v$  then
2:    $d(u, v) \leftarrow \hat{d}(u, v)$ ,  $\mathcal{P}(u, v) \leftarrow \{(u, v)\}$ 
3:   return  $(\hat{d}(u, v), \mathcal{P}(u, v))$ 
4: else
5:   Construct a weighted directed graph  $G = (\mathcal{C} \cup \{u, v\}, E; w)$  where
       $E \triangleq \{ \{u, z\} : z \in \mathcal{C}, \hat{d}(u, z) \leq U - d''_u \} \cup \{ \{v, z\} : z \in \mathcal{C}, \hat{d}(v, z) \leq U - d'_v \} \cup \{ \{z, z'\} : z, z' \in \mathcal{C}, \hat{d}(z, z') \leq U \}$ 
      and  $w(z, z') \triangleq \hat{d}(z, z')$  for all  $z, z' \in \mathcal{C} \cup \{u, v\}$ 
6:    $\mathcal{P}(u, v) \leftarrow$  shortest path between  $u$  and  $v$  in  $G$  (with a set of edge
      lengths  $\{w(u, v)\}_{u,v}$ )
7:    $\hat{d}(u, v) \leftarrow$  length of  $\mathcal{P}(u, v)$ 
8:   return  $(\hat{d}(u, v), \mathcal{P}(u, v))$ 
9: end if

```

---

## B. Extensions

The preceding section presents a basic setting of DFP and its efficient algorithms. In reality, an automated drone management system requires more sophisticated options. In this section, we present two extensions to the preceding algorithms to obtain heuristics for more practical scenarios.

---

**Algorithm 3** Fix-plan $[G, \mathcal{F}_0]$ 


---

```

1:  $\mathcal{F} \leftarrow \emptyset$ 
2: for each  $(u, v)$  in  $\mathcal{F}_0$  do
3:   Add  $\mathcal{P}(u, v)$  to  $\mathcal{F}$ 
4: end for
5: Add to  $\mathcal{F}$  a set of sub-tours  $\{(u, s'_u), (s'_u, s''_u), (s''_u, u) : u \in V\}$ 
6: for  $u \in V$  do
7:   if  $\mathcal{F} \setminus \{(u, s'_u), (s'_u, s''_u), (s''_u, u)\}$  is feasible then
8:      $\mathcal{F} \leftarrow \mathcal{F} \setminus \{(u, s'_u), (s'_u, s''_u), (s''_u, u)\}$ 
9:   end if
10: end for
11: return  $\mathcal{F}$ 

```

---

**Algorithm 4** Fix-charge $[\mathcal{F}, b(\cdot)]$ 


---

```

1: Let  $\mathcal{F}_{i_1}, \dots, \mathcal{F}_{i_r}$  be the charging stations, in the order they appear on  $\mathcal{F}$ 
2: for  $j = 0, 1, \dots, r$  do
3:    $D_j = \eta_d \sum_{k=i_j}^{i_{j+1}-1} c_f(\mathcal{F}_k, \mathcal{F}_{k+1}) d(\mathcal{F}_k, \mathcal{F}_{k+1})$ 
4: end for
5: for  $j = 1, \dots, r$  do
6:    $B_j \triangleq \eta_c \sum_{k=1}^j b(\mathcal{F}_{i_k})$ 
7: end for
8: for  $j = r$  downto 1 do
9:    $b'(\mathcal{F}_{i_j}) = \max\{0, \frac{1}{\eta_c} (\underline{B} - x_0 + \sum_{k=0}^r D_k - \sum_{k=1}^{j-1} B_k)\}$ 
10:  if  $b'(\mathcal{F}_{i_j}) > 0$  then
11:    exit
12:  end if
13: end for
14: return  $b'(\cdot)$ 

```

---

1) *Wind Uncertainty*: Under steady wind condition, we assume in the preceding algorithms that  $c_f(u, v)$  is a constant that depends on the designated path between sites  $u$  and  $v$ . In practice, there is sometimes uncertainty in the wind condition. Often, the wind varies as the drone flies. This also depends on the expected wind condition on this path. Thus, it should be more precisely represented by  $c_f(u, v, w)$ , where  $w$  is the wind vector whose value is in an uncertain domain  $w \in W$ . For example,  $W$  is defined by the predicted speed range  $[\|w\|, \bar{w}\|]$  and the predicted orientation range  $[\theta_w, \bar{\theta}_w]$ . We can modify the algorithms to account for the uncertainty of  $W$ . We proceed conservatively in our algorithm by taking the worst-case, replacing  $c_f(u, v)$  by  $\bar{c}_f(u, v) = \max_{w \in W} c_f(u, v, w)$ .

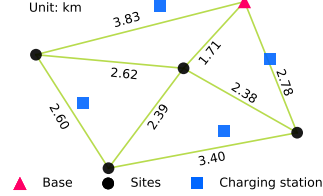
2) *Variable Drone Speed*: We consider another scenario, in which the drone can vary its speed uniformly at all designated paths in  $V$ . In this case, we run our algorithms sequentially in multiple rounds, with an increasing drone speed at each round, until the algorithms can not return a feasible solution (because that higher drone speed may result in insufficient battery to reach some sites). Then we will enumerate all the optimal solutions in all the rounds to find the best solution with the lowest total flight time. By enumerating the possibilities of different drone speeds, the algorithms can identify an optimal flight mission plan.

## VI. EXPERIMENTAL VALIDATION AND CASE STUDIES

We implemented the algorithms in an automated drone management system. In particular, we evaluated the results of flight mission planning and recharging optimization for the test drones in a real-world experiment, and several case studies, based on the data from empirical studies.

### A. Simulation: Case Studies

**Setup.** We considered a scenario with four sites of interest, and four charging stations. The drone is programmed to begin its mission from the base. Fig. 9 depicts the geographical locations of the sites (as black points), charging stations (as blue squares) and the base (as magenta triangle). The choices of geographical locations and distances are based on some real locations of a suburban community.



Case	Battery (Wh)	$\ \vec{w}_{xy}\ $ (km/h)	$m$ (g)
1	70	20	0
2	70	North-East	0
3	140	South	500
4	140	North-East	500

TABLE II: Parameters of setup.

Fig. 9: Geographical locations of sites.

There are two major sets of studies conducted as follows.

- 1) *Study 1*: We study 4 cases as follows. We consider using one battery in the first two cases of each drone. Different wind conditions with average wind speed of 18 km/h were studied in the cases. Then we double the battery capacity with the same wind condition in another two cases. Since the battery capacity was doubled, extra weight was added to the drone. The parameters of all the cases are summarized in Table II. The cases are denoted by  $S_1C_1$  to  $S_1C_4$
- 2) *Study 2*: We consider uncertainty of wind conditions. The wind speed and orientation varied within a certain range. The wind speed varied from 0 to 21 km/h in four discrete scales, while the wind orientation varies from  $0^\circ$  to  $360^\circ$  in four discrete scales. The cases are denoted by  $S_2C_1$  to  $S_2C_4$ ,

**Results.** For comparison, we also considered a *benchmark* algorithm, by which a drone flew to the nearest unvisited site, or the SoC dropped below a preset threshold, then the drone flies to a charging station instead. We set the preset threshold to be the minimum SoC that could fly to a nearest charging station from any site.

- 1) *Study 1*:

Fig. 10 visualizes the results of Simulation 1. The numbers indicate the path order of the drone. The colors represent the SoC of battery. The wind orientations are displayed on the upper-left corners.

We plot the travel time and energy consumption of Simulation 1 in Fig. 12. We normalize the travel time and energy consumption by the results of  $S_1C_1$  (i.e., the lowest travel time and energy consumption), as listed in Table III. There are two observations:

- The north-east wind causes higher energy consumption than that by south wind. Besides, higher travel time is observed due to longer charging time.
- Increasing battery capacity for 3DR Solo drone does not help to reduce the travel time. We observe that even the flying time in  $S_1C_3$  is the shortest, it takes more time to charge since the drone becomes

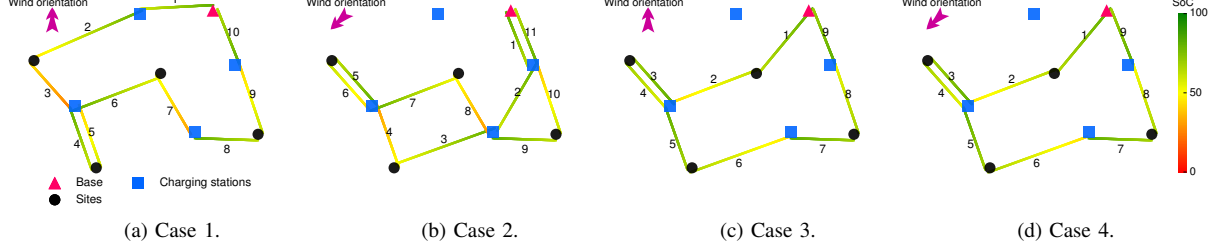


Fig. 10: Visualized results of Simulation 1.

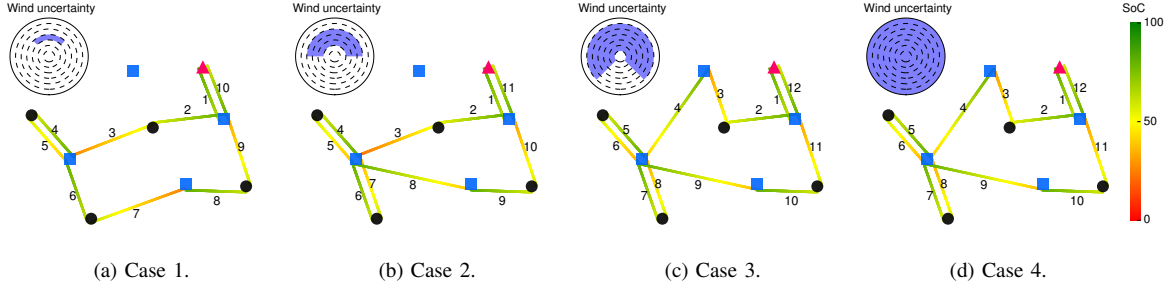


Fig. 11: Visualized results of Simulation 2.

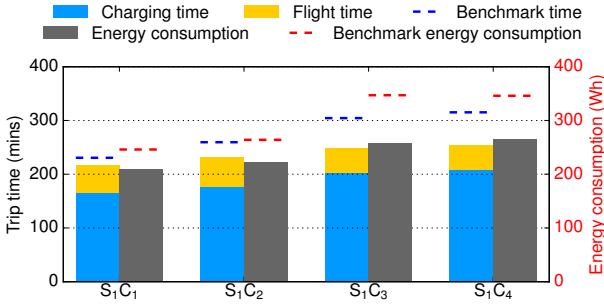


Fig. 12: Results of Simulation 1.

heavier by carrying extra weight for the battery, which results in longer travel time.

	S <sub>1</sub> C <sub>1</sub>	S <sub>1</sub> C <sub>2</sub>	S <sub>1</sub> C <sub>3</sub>	S <sub>1</sub> C <sub>4</sub>
Travel Time	1	1.07	1.15	1.20
Energy Consumption	1	1.07	1.24	1.48

TABLE III: Comparisons of results

## 2) Study 2:

Fig. 11 visualizes the results of Simulation 2. The numbers indicate the path order for the drone. We represent the ranges of wind speeds and orientations as the shaded areas on the upper-left corners. We plot the travel time and energy consumption of Simulation 2 in Fig. 13.

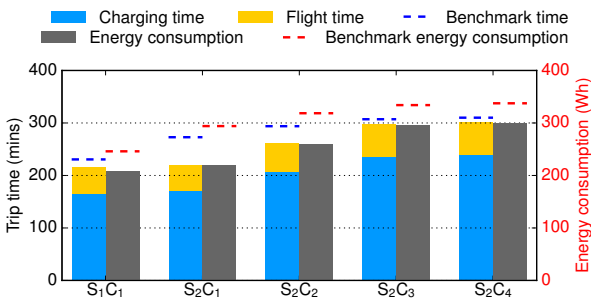


Fig. 13: Results of Simulation 2.

The energy consumption of S<sub>1</sub>C<sub>1</sub> is the result without

uncertain wind condition for the 3DR solo drone with 70 Wh battery. In Simulation 2, we study if a solution can be obtained in the presence of uncertainty of wind condition. We gradually increase the uncertainty from S<sub>2</sub>C<sub>1</sub> to S<sub>2</sub>C<sub>4</sub>. For example, in S<sub>2</sub>C<sub>1</sub> the wind speed varies from 9 to 12 km/h and orientation varies from -45° to 45°. We observe that the energy consumption increases as the uncertainty of wind condition increases in Fig. 13. The energy consumption of the worst uncertainty is in S<sub>2</sub>C<sub>4</sub>, in which the drone may always fly into a tailwind. S<sub>2</sub>C<sub>4</sub> provides the most conservative result.

## B. Simulation: Scalability

To showcase the algorithm's performance and scalability, we tested against randomly generated large instances with up to two hundred vertices. The number of charging stations is set to one-fifth of the number of vertices, while the remaining are sites of interest. All vertices are positioned uniformly at random on a canvas area of 3.33 km by 3.33 km. We set drone speed at 18 km/h, battery capacity to 80 Wh and uniformly random wind speed within a range of [0, 3.6] km/h with a direction of 225°, with a uniform uncertainty of 10° degrees.

Fig 14a plots the *empirical* and *theoretical* approximation ratio of Alg. 3 at 95% confidence interval. In order to compute the approximation ratios, an exact ILP formulation of the problem was used to represent the optimal solution. The Figure shows that the *empirical* approximation ratio always remains below the theoretical ratio. Furthermore, the empirical ratio slightly decreases as we increase the number of vertices, while the *theoretical* approximation ratio increases due to the log component of the approximation guarantee (in the proof of Theorem 1).

Fig. 14b shows the running time of Alg. 3 (implemented in Python 3 on an Intel i9-9900k CPU with 32 GB of

RAM) along with the total *energy savings* of the solution after invoking recharging optimization (Alg. 4). Although our implementation is not optimal (written in Python 3), the algorithm's running time scales reasonably well to more than 200 vertices. Furthermore, we observe the energy savings are more significant with a lower number of vertices, primarily due to the diminishing return of partially charging the battery at certain charging stations (Alg. 4).

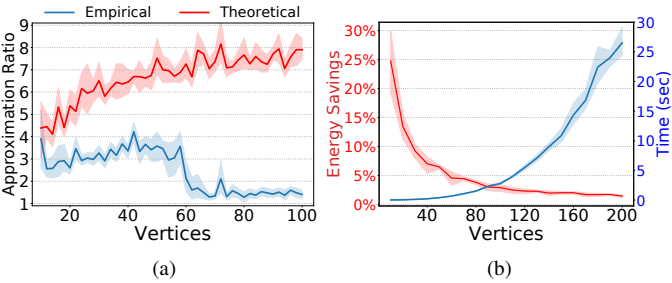


Fig. 14: The algorithm's performance against the number of vertices at 95% confidence interval: (a) approximation ratio, (b) running time and charging optimization savings percentage.

### C. Real-World Experiment

To evaluate the route feasibility of our approach in a real-world environment, we utilized the DJI Matrice 600 drone, which has a maximum flight duration of 38 minutes and a payload capacity of 6 kg. The drone was equipped with a 2 kg payload. The experiment setup, illustrated in Fig. 15, includes a start and endpoint, four waypoints, and a charging station. The computed route by Alg. 3 has a total travel distance of 9.47 km. The algorithm parameters we set to 30 km/h horizontal speed, and an estimated wind speed of 30 km/h, and 120-meter altitude.

Fig. 16 shows the experiment's expected and actual battery capacity throughout the route provided by the algorithm, [S, 1, 2, 3, C, 4, S]<sup>3</sup>, in which it recharges once. The red line shows a lower bound on the battery at 40%. Vertical green dashed lines represent sites of interest, whereas the dashed blue line represents a charging station. We observe a small difference between the actual battery energy level and the estimated one. This has been primarily due to our inaccurate wind model, which was based solely on the start point. Thus, to avoid infeasible routes, one can increase the minimum battery energy level (e.g., 40%) or use a more accurate wind model by installing multiple sensors in the region of interest.

## VII. AUTOMATED DRONE MANAGEMENT SYSTEM

### A. User Interface

We implemented our algorithms in an automated drone management system. The user interface of our system is depicted in Fig 17. The user interface allows the users to specify individual goals and to visualize the computed flight mission plan. The system connects to a cloud computing server, which

<sup>3</sup>The start point was at coordinates 25°13'7.1796" N, 55°39'37.8972" E. See a video footage of the experiment at <https://bit.ly/3h1UOus>.



Fig. 15: The experiment's route for DJI Matrice 600. S is the starting and finishing points and C is the charging station.

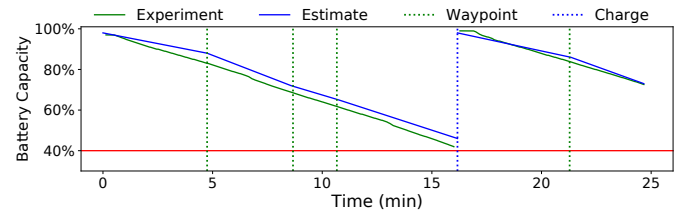


Fig. 16: The experiment's power consumption, and estimation.

accepts location data from the users and computes the optimal flight mission plan. Then the drone is programmed to follow the pre-computed flight mission plan.

Furthermore, a dynamic tracking system of drone using onboard sensors, including GPS location, video feed, and SoC, can monitor the real-time flight status of the drone. If deviant measurements are detected, for example, the reported sensor measurements deviating from the estimated value from pre-computed flight mission, then re-computation will be performed to obtain the adjusted flight mission. Users can also abort the flight mission through the system.

### B. Robotic Charging System

Complementary to the automated drone management system, we also developed a robotic charging system that can recharge drones autonomously. In robotic charging system, there is a tethered rover that is capable of autonomous navigation, and is equipped with a robotic arm carrying a charging pad that can reach to different drones and positions (see Fig. 18). Our

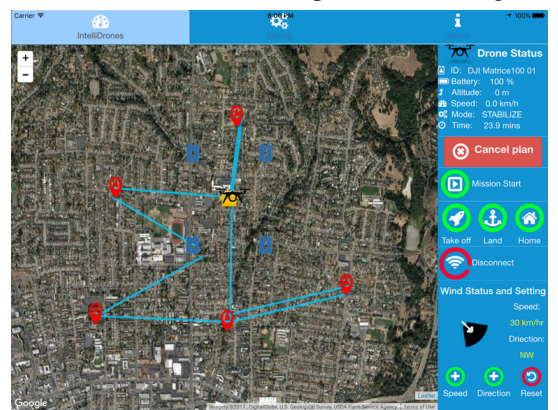


Fig. 17: User interface of drone management system.

robotic rover uses 2D Light Detection and Ranging (LIDAR) sensors to navigate and detect the presence of a drone.

A retractable robotic arm is used to conduct inductive charging for the drones, which can flexibly recharge drones in arbitrary positions. The inductive charging technology is based on resonant inductive coupling, which can transfer energy without physical contact. It has been widely used in wireless charging systems for smart phones. The use of inductive charging technology facilitates a fully automated drone management system, without the need to manually connect to an external charger. The robotic charging system employs six coils for inductive charging, giving a maximum charging current of  $6 \times 700 = 3500$  mA. We also mounted six current sensors on the robotic arm to measure individual coil charging rate. Our test drone is DJI Matrice 100 which is powered by two 5700 mA on-board Li-Poly battery. More details of robotic charging station can be found in [28].

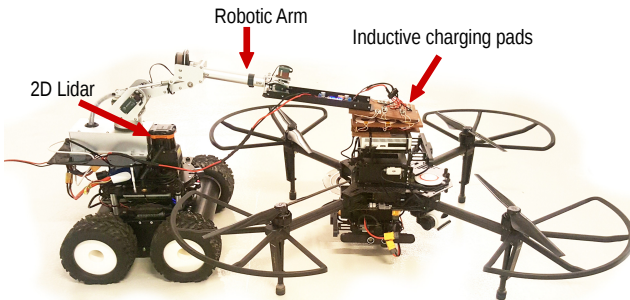


Fig. 18: Robotic charging system.

## VIII. CONCLUSION

Automated drone management system is important for practical applications of drones. This paper provides multiple contributions to automated management systems for battery-operated drones, including empirical studies to model the battery performance of drones considering various flight scenarios, a study of flight mission planning and recharging optimization for drones that captures diverse applications of delivery and remote operations by drones, and a management system implementation with a robotic charging station to support autonomous recharging of drones.

In future work, we will incorporate a variety of further features in our automated drone management system, such as restrictions of no-fly zones and attitude, and wind speed forecast. Users may also be able to specify further goals, such as deadline of completion and maximum payload weight.

## REFERENCES

- [1] K. Nonami, F. Kendoul, S. Suzuki, W. Wang, and D. Nakazawa, Eds., *Autonomous Flying Robots: Unmanned Aerial Vehicles and Micro Aerial Vehicles*. Springer Publisher, 2010.
- [2] Y. B. Sebbane, Ed., *Smart Autonomous Aircraft: Flight Control and Planning for UAV*. CRC Press, 2015.
- [3] J. K. Stolaroff, C. Samaras, E. R. O'Neill, A. Lubers, A. S. Mitchell, and D. Ceperley, "Energy use and life cycle greenhouse gas emissions of drones for commercial package delivery," *Nature Communications*, vol. 9, 2018.
- [4] S. H. Kim, "Third-party risk of mid-air collision between small unmanned aircraft systems," in *AIAA Aviation 2019 Forum*, 2019, p. 3052.
- [5] A. Otto, N. Agatz, J. Campbell, B. Golden, and E. Pesch, "Optimization approaches for civil applications of unmanned aerial vehicles (uavs) or aerial drones: A survey," *Networks*, vol. 72, no. 4, pp. 411–458, 2018.
- [6] K. Sundar and S. Rathinam, "Algorithms for routing an unmanned aerial vehicle in the presence of refueling depots," *IEEE Trans. Automation Science and Engineering*, vol. 11, no. 1, pp. 287–294, 2013.
- [7] K. Dorling, J. Heinrichs, G. G. Messier, and S. Magierowski, "Vehicle Routing Problems for Drone Delivery," *IEEE Trans. Systems, Man, and Cybernetics: Systems*, vol. 47, no. 1, pp. 70–85, 2017.
- [8] B. D. Song, K. Park, and J. Kim, "Persistent UAV delivery logistics: MILP formulation and efficient heuristic," *Computers & Industrial Engineering*, vol. 120, pp. 418–428, 2018.
- [9] J. Shao, J. Cheng, B. Xia, K. Yang, and H. Wei, "A Novel Service System for Long-Distance Drone Delivery Using the Ant Colony+A\* Algorithm," *IEEE Systems Journal*, pp. 1–12, 2020.
- [10] R. G. Ribeiro, J. R. C. Júnior, L. P. Cota, T. A. M. Euzébio, and F. G. Guimarães, "Unmanned Aerial Vehicle Location Routing Problem With Charging Stations for Belt Conveyor Inspection System in the Mining Industry," *IEEE Trans. Intelligent Transportation Systems*, vol. 21, no. 10, pp. 4186–4195, 2020.
- [11] M. Torabbeigi, G. J. Lim, and S. J. Kim, "Drone delivery scheduling optimization considering payload-induced battery consumption rates," *Journal of Intelligent & Robotic Systems*, vol. 97, no. 3, pp. 471–487, Mar 2020.
- [12] C. Cheng, Y. Adulyasak, and L.-M. Rousseau, "Drone routing with energy function: Formulation and exact algorithm," *Transportation Research Part B: Methodological*, vol. 139, pp. 364–387, 2020.
- [13] S. Bouabdallah, A. Noth, and R. Siegwart, "PID vs LQ control techniques applied to an indoor micro quadrotor," in *IROS*, 2004.
- [14] E. Bregu, N. Casamassima, L. Mottola, and K. Whitehouse, "Reactive control of autonomous drones," in *ACM MobiSys*, 2016.
- [15] R. Siegwart, I. Nourbakhsh, and D. Scaramuzza, *Introduction to Autonomous Mobile Robots*. MIT Press, 2015.
- [16] T. Ji, S. Chen, R. Varma, and J. Kovacevic, "Energy-efficient route planning for autonomous aerial vehicles based on graph signal recovery," in *ALLERTON*, 2015.
- [17] E. Kim, J. Lee, and K. G. Shin, "Real-time prediction of battery power requirements for electric vehicles," in *IEEE/ACM ICCPS*, 2013.
- [18] A. Cappiello, I. Chabini, E. K. Nam, A. Lue, and M. A. Zed, "A statistical model of vehicle emissions and fuel consumption," in *IEEE Intelligent Transportation Systems Conf.*, 2002.
- [19] H. X. Li and B. C. Williams, "Generative planning for hybrid systems based on flow tubes," in *ICAPS*, 2008, pp. 206–213.
- [20] A. Coles, M. Fox, D. Long, and A. Smith, "Planning with problems requiring temporal coordination," in *AAAI*, 2008, pp. 892–897.
- [21] E. Fernandez-Gonzalez, B. Williams, and E. Karpas, "Scottyactivity: Mixed discrete-continuous planning with convex optimization," *Journal of Artificial Intelligence Research*, vol. 62, pp. 579–664, 2018.
- [22] M. Ono, B. C. Williams, and L. Blackmore, "Probabilistic planning for continuous dynamic systems under bounded risk," *Journal of Artificial Intelligence Research*, vol. 46, pp. 511–577, 2013.
- [23] M. Lv, N. Guan, Y. Ma, D. Ji, E. Knipper, X. Liu, and W. Yi, "Speed planning for solar-powered electric vehicles," in *ACM e-Energy*, 2016.
- [24] C.-K. Chau, K. Elbassioni, and C.-M. Tseng, "Drive mode optimization and tour planning for plug-in hybrid electric vehicles," *IEEE Trans. Intell. Transp. Syst.*, 2017.
- [25] S. Khuller, A. Malekian, , and J. Mestre, "To fill or not to fill: The gas station problem," *ACM TALG*, vol. 7, pp. 534–545, 2011.
- [26] A. M. Frieze, G. Galbiati, and F. Maffioli, "On the worst-case performance of some algorithms for the asymmetric traveling salesman problem," *Networks*, vol. 12, no. 1, pp. 23–39, 1982.
- [27] P. K. Chittoor, B. Chokkalingam, and L. Mihet-Popa, "A review on uav wireless charging: Fundamentals, applications, charging techniques and standards," *IEEE Access*, vol. 9, pp. 69 235–69 266, 2021.
- [28] M. Khanji, M. Alshehhi, C.-M. Tseng, and C.-K. Chau, "Autonomous inductive charging system for battery-operated electric drones," in *ACM EV-Sys*, 2017.
- [29] 3DR Solo, <https://3dr.com/solo-drone/specs/>, 2017.
- [30] DJI Matrice 100, <https://www.dji.com/matrice100/info>, 2017.
- [31] DJI Matrice 600 Pro, <https://www.dji.com/ae/matrice600-pro>, 2021.
- [32] H. F. Handbook. US Federal Aviation Administration, 2012.
- [33] R. K. Ganti, N. Pham, H. Ahmadi, S. Nangia, and T. F. Abdelzaher, "GreenGPS: a participatory sensing fuel-efficient maps application," in *ACM MobiSys*, 2010.
- [34] S. Grubwinkler and M. Lienkamp, "A modular and dynamic approach to predict the energy consumption of electric vehicles," in *Conf. Future Automotive Technology*, 2013.
- [35] C.-M. Tseng, C.-K. Chau, S. Dsouza, and E. Wilhelm, "A participatory sensing approach for personalized distance-to-empty prediction and green telematics," in *ACM e-Energy*, 2015.

- [36] C.-M. Tseng and C.-K. Chau, "Personalized prediction of vehicle energy consumption based on participatory sensing," *IEEE Trans. Intell. Transp. Syst.*, 2017.

## APPENDIX

### A. Details of Test Drones

	3DR Solo	DJI Matrice 100	DJI Matrice 600
Weight	2 kg	2.8 kg	9.1 kg
Dimensions	25cm × 46cm	46cm × 46cm	166.8cm × 151.8cm
Battery	5200 mAh 14.8V	5700 mAh 22.8V	4500 mAh 22.2V (×6)
Battery Weight	500 g	600 g	595 g(×6)
Motors	880 kV (×4)	350 kV (×4)	130 kV (×6)
Max Speed	20 km/h	60 km/h	65 km/h
Max Altitude	122 ft (FAA)	122 ft (FAA)	122 ft (FAA)
Charging Duration	90 mins	180 mins	92 mins
Software	Python Dev Kit	DJI SDK & ROS	DJI SDK & ROS

TABLE IV: Specifications of test drones.

### B. Proofs

**Lemma 1.** In an optimal flight mission plan  $(\mathcal{F}, b(\cdot))$ , we have

$$\underline{c} \cdot d(\mathcal{F}) + c' \leq \tau(\mathcal{F}) + \tau_c(b(\mathcal{F})) \leq \bar{c} \cdot d(\mathcal{F}) + c'$$

where either

- 1)  $\underline{c} = \bar{c} = c_a$  and  $c' = 0$ , or
- 2)  $\underline{c} = c_a + \underline{c}_f c_b \frac{\eta_d}{\eta_c}$ ,  $\bar{c} = c_a + \bar{c}_f c_b \frac{\eta_d}{\eta_c}$ , and  $c' = \frac{c_b}{\eta_c} (\underline{B} - x_0)$ .

*Proof.* Consider an optimal flight plan  $(\mathcal{F}, b(\cdot))$  and assume that the charging stations, in the order they appear on  $\mathcal{F}$ , is  $\mathcal{F}_{i_1}, \dots, \mathcal{F}_{i_r}$ , where without loss of generality, we assume  $\mathcal{F}_{i_1} \neq v_0$ . For completeness, let  $i_0 \triangleq 1$  and  $i_{r+1} \triangleq |\mathcal{F}|$ . For  $j = 0, 1, \dots, r$ , let

$$D_j \triangleq \eta_d \sum_{k=i_j}^{i_{j+1}-1} c_f(\mathcal{F}_k, \mathcal{F}_{k+1}) \cdot d(\mathcal{F}_k, \mathcal{F}_{k+1}),$$

and for  $j = 1, \dots, r$ , let  $B_j \triangleq \eta_c b(\mathcal{F}_{i_j})$ .

Then, the feasibility of the flight mission plan  $\mathcal{F}$  implies

$$I(r) \triangleq x_0 - \sum_{k=0}^j D_k + \sum_{k=1}^j B_k \geq \underline{B}, \text{ for } j = 0, \dots, r \quad (13)$$

Let us refer to Ineq. (13) for a particular  $j$  as  $I(j) \geq \underline{B}$ . Particularly, consider  $I(r) \geq \underline{B}$ . Suppose that this inequality is not tight, that is, the left-hand side is strictly larger than the right-hand side. Note that the variable  $b(\mathcal{F}_{i_r}) = \frac{\underline{B}_r}{\eta_c}$  appears only in this inequality. Since  $b(\mathcal{F}_{i_r})$  appears in the objective function  $\tau_c(b(\mathcal{F}))$  with a positive coefficient (i.e.,  $\tau_c(b(u)) = c_b b(u)$ ), there are two cases: (i)  $b(\mathcal{F}_{i_r}) = 0$  at optimality, if  $I(r) > \underline{B}$ , or (ii)  $b(\mathcal{F}_{i_r}) > 0$  at optimality, if  $I(r) = \underline{B}$ . Otherwise, it will contradict to the optimality of  $b(\mathcal{F}_{i_r})$ , by reducing the value of  $b(\mathcal{F}_{i_r})$ . If it is case (i), then the inequality  $I(r-1) \geq \underline{B}$  becomes redundant (as  $I(r-1) \geq I(r) > 0$ ). Removing  $I(r-1) \geq \underline{B}$ , the variable  $b(\mathcal{F}_{i_{r-1}})$  appears only in  $I(r) \geq \underline{B}$ . Similarly, we conclude that  $b(\mathcal{F}_{i_{r-1}}) = 0$  and remove the (now) redundant inequality  $I(r-2) \geq \underline{B}$ .

Continuing this argument, we conclude that there are two cases: (1) either all variables  $b(\mathcal{F}_{i_j})$  are set to zero in which case the value of the objective is  $\tau(\mathcal{F}) = c_a d(\mathcal{F})$ , or (2) we have

$$x_0 - \sum_{k=0}^r D_k + \sum_{k=1}^r B_k = \underline{B},$$

In case (2), the value of the objective is

$$\begin{aligned} \tau(\mathcal{F}) + \frac{c_b}{\eta_c} \sum_{k=1}^r B_k &= \tau(\mathcal{F}) + \frac{c_b}{\eta_c} (\underline{B} - x_0 + \sum_{k=0}^r D_k) \\ &= \tau(\mathcal{F}) + \frac{c_b}{\eta_c} \sum_{k=0}^r D_k + \frac{c_b}{\eta_c} (\underline{B} - x_0) \end{aligned}$$

Therefore,

$$\begin{aligned} &\left( c_a + \underline{c}_f c_b \frac{\eta_d}{\eta_c} \right) d(\mathcal{F}) + \frac{c_b}{\eta_c} (\underline{B} - x_0) \\ &\leq \tau(\mathcal{F}) + \frac{c_b}{\eta_c} \sum_{k=0}^r D_k + \frac{c_b}{\eta_c} (\underline{B} - x_0) \\ &\leq \left( c_a + \bar{c}_f c_b \frac{\eta_d}{\eta_c} \right) d(\mathcal{F}) + \frac{c_b}{\eta_c} (\underline{B} - x_0). \end{aligned}$$

□

**Lemma 2.** Given any feasible flight mission plan  $(\mathcal{F}, b(\cdot))$ , there is another feasible flight mission plan  $(\mathcal{F}, b'(\cdot))$  such that

$$\tau_c(b(\mathcal{F})) \leq \frac{\underline{B} - x_0}{\eta_c} + \frac{\bar{c}_f \eta_d}{\eta_c} \cdot d(\mathcal{F})$$

Such a plan  $(\mathcal{F}, b'(\cdot))$  can be found in  $O(|V|)$  time.

*Proof.* The proof follows from Lemma 1, which uses algorithm Fix-charge to implement the argument used in Lemma 1 to find a feasible flight mission plan. □

**Theorem 1.** The flight plan  $(\mathcal{F}, b'(\cdot))$  returned by algorithm Find-plan[V, d] has cost

$$\tau(\mathcal{F}) + \tau_c(b(\mathcal{F})) = O(\text{OPT}_{\text{DFP}}) + O(1).$$

*Proof.* Let  $(\mathcal{F}^*, b^*(\cdot))$  be an optimal flight plan for (DFP). Clearly, this plan can be trivially turned into a feasible solution  $(\mathcal{F}^*, x)$  for (SDFP) by setting  $x_k = \underline{B}$  for all  $\mathcal{F}_k \in \mathcal{C}$ . It follows that

$$\text{OPT}_{\text{SDFP}} \leq \widehat{d}(\mathcal{F}^*). \quad (14)$$

On the other hand, Lemma 3 implies that

$$\widehat{d}(\mathcal{F}) \leq \left( \frac{(1 + \alpha + \alpha\beta) \log(|T|)}{1 - \alpha} \right) \text{OPT}_{\text{SDFP}}. \quad (15)$$

Lemma 1 also implies that

$$\text{OPT}_{\text{DFP}} \geq \underline{c} \cdot d(\mathcal{F}^*) + c', \quad (16)$$

while Lemma 2 implies that

$$b(\mathcal{F}) \leq \frac{\underline{B} - x_0}{\eta_c} + \frac{\bar{c}_f \eta_d}{\eta_c} d(\mathcal{F}), \quad (17)$$

and the definition of  $\widehat{d}(\cdot, \cdot)$  implies

$$\underline{c}_f d(\mathcal{F}) \leq \widehat{d}(\mathcal{F}) \text{ and } \widehat{d}(\mathcal{F}^*) \leq \bar{c}_f d(\mathcal{F}^*). \quad (18)$$

Putting together (14), (15), (16), (17), and (18), we obtain

$$\begin{aligned} \tau(\mathcal{F}) + \tau_c(b(\mathcal{F})) &= c_a d(\mathcal{F}) + c_b b(\mathcal{F}) \\ &\leq \left( c_a + \underline{c}_f c_b \frac{\eta_d}{\eta_c} \right) d(\mathcal{F}) + c_b \frac{\underline{B} - x_0}{\eta_c} \\ &\leq \left( \frac{(1 + \alpha + \alpha\beta) \log(|T|)}{1 - \alpha} \right) \frac{\bar{c}_f}{\underline{c}_f} \left( c_a + \bar{c}_f c_b \frac{\eta_d}{\eta_c} \right) \left( \frac{\text{OPT}_{\text{DFP}} - c'}{\underline{c}} \right) + c_b \frac{\underline{B} - x_0}{\eta_c} \end{aligned}$$

□